Machine Learning Unveils the Power Law of Finite-Volume Energy Shifts

Weijie Zhang[1,2,3†], Zhenyu Zhang[1,2,3†], Jifeng Hu[1,3], Bingnan Lu[4], Jinyi Pang[5], and Qian Wang[1,3,6,7*]

[1]*State Key Laboratory of Nuclear Physics and Technology, Institute of Quantum Matter, South China Normal University, Guangzhou 510006, China*
[2]*Key Laboratory of Atomic and Subatomic Structure and Quantum Control (MOE), Guangdong–Hong Kong Joint Laboratory of Quantum Matter, Guangzhou 510006, China*
[3]*Guangdong Basic Research Center of Excellence for Structure and Fundamental Interactions of Matter, Guangdong Provincial Key Laboratory of Nuclear Science, Guangzhou 510006, China*
[4]*Graduate School of China Academy of Engineering Physics, Beijing 100193, China*
[5]*College of Science, University of Shanghai for Science and Technology, Shanghai 200093, China*
[6]*Southern Center for Nuclear-Science Theory, Institute of Modern Physics, Chinese Academy of Sciences, Huizhou 516000, China*
[7]*Research Center for Nuclear Physics, Osaka University, Ibaraki 567-0047, Japan*

(Received 12 April 2025; accepted manuscript online 29 May 2025)

Finite-volume extrapolation is an important step for extracting physical observables from lattice calculations. However, it is a significant challenge for systems with long-range interactions. We employ symbolic regression to regress the finite-volume extrapolation formula for both short-range and long-range interactions. The regressed formula still holds the exponential form with a factor L^n in front of it. The power decreases with the decreasing range of the force. When the range of the force becomes sufficiently small, the power converges to -1, recovering the short-range formula as expected. Our work represents a significant advancement in leveraging machine learning to probe uncharted territories within particle physics.

DOI: 10.1088/0256-307X/42/7/070202 CSTR: 32039.14.0256-307X.42.7.070202

1. Introduction. Lattice quantum chromodynamics, which discretizes space into a four-dimensional hypercubic lattice and performs the calculations in a given finite volume, is a foundational computational framework for studying strong interactions. It predicts not only the spectrum of conventional hadrons but also reveals the existence of exotic hadronic states. In particular, it has recently provided precise calculations for near-threshold states, taking the double charm tetraquark as an example.[1–3] To extract physical observables from lattice calculations, finite-volume extrapolation is essential. However, the presence of long-range interactions presents significant challenges, as they invalidate key assumptions underlying standard approaches, most notably the Lüscher formula.[4] When light particles mediate forces between scattering states, conventional methods may fail, leading to uncontrolled systematic uncertainties. Addressing these issues is crucial for reliable lattice analyses, particularly in systems where long-range effects play a dominant role, such as one-pion exchange in nucleon–nucleon scattering and the effects of light-meson exchange in the D^*D system.[5] Recent theoretical studies[6–10] try to solve this problem by either modifying the Lüscher formula numerically, but without an explicit formula as simple as that for the short-range interaction,[11] or performing quantization conditions using a plane-wave basis.[12] Moreover, understanding finite-volume effects in two-body systems with long-range interactions is a necessary step towards addressing similar challenges in three-body systems.

Fortunately, deriving fundamental mathematical expressions directly from empirical data[13] is an advantage of symbolic regression,[14] which has exhibited its capability in physics and scientific research.[15] Unlike traditional regression, it automatically discovers interpretable laws by exploring vast expression spaces. This has enabled the rediscovery of known physical laws and the formulation of novel equations for complex systems,[16] even when their underlying principles are elusive. Recent advances in symbolic regression enhance its effectiveness by incorporating physical constraints like dimensional consistency, thus improving search efficiency and model plausibility. For example, the AI Feynman algorithm has derived 100 equations from the Feynman Lectures on Physics.[17] Its ability to generate human-readable models accelerates discovery across various fields.[18,19] For instance, in high-energy physics, it has revealed fundamental distributions, such as the Tsallis distribution in hadron transverse momentum analysis.[20] Moreover, it has provided analytical expressions for key low-energy observables, including the Higgs mass, muon anomalous magnetic moment, and dark matter relic density.[21] Reference [22] uses neural network to reproduce the numerical Lüscher's formula to a high precision.

†These authors contributed equally to this work.
*Corresponding author. Email: qianwang@m.scnu.edu.cn
© 2025 Chinese Physical Society and IOP Publishing Ltd. All rights, including for text and data mining, AI training, and similar technologies, are reserved.

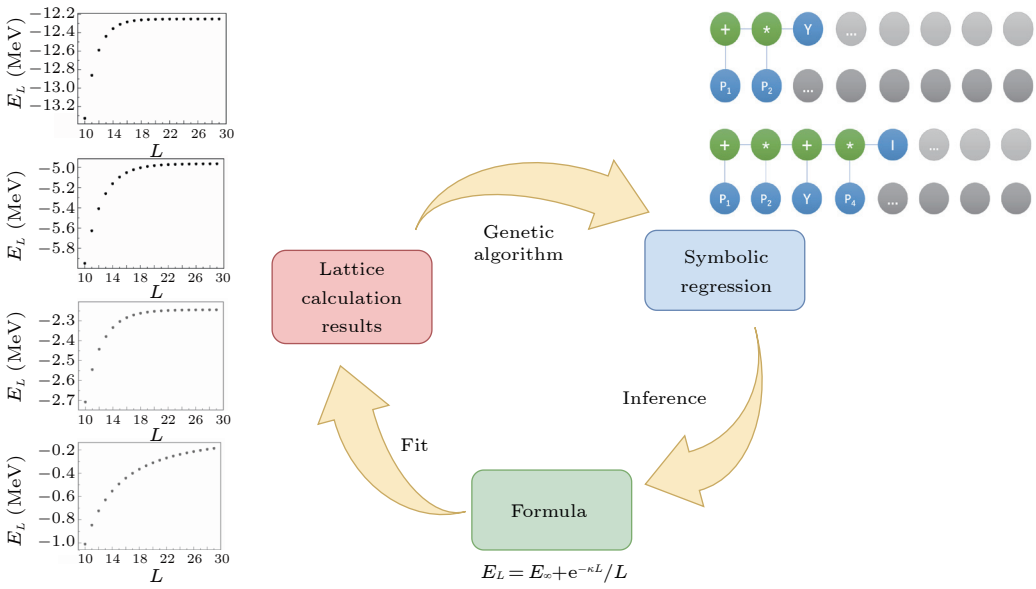

Fig. 1. Workflow of using symbolic regression, LEFT, and formula.

As a result, we employ symbolic regression to probe the finite-volume extrapolation formula for long-range interactions. Before symbolic regression, we need to prepare samples for training symbolic regression. For these samples, we borrow the hadron lattice effective field theory (HLEFT),[23] which is analogous to the nuclear lattice effective field theory (NLEFT), a powerful computational framework for *ab initio* nuclear structure calculations.[24] The approach implements a systematic discretization of nucleon–nucleon interactions on a three-dimensional cubic lattice with periodic boundary conditions. These quantum many-body systems are subsequently solved using advanced numerical techniques including the Lanczos diagonalization method and auxiliary field Monte Carlo simulations. NLEFT has demonstrated remarkable success across diverse domains of nuclear physics, particularly in characterizing nuclear ground states[25–31] and excited states,[32–35] elucidating nuclear intrinsic density distributions and clustering phenomena,[36–40] analyzing nucleus–nucleus scattering processes,[41,42] and investigating both zero-temperature and finite-temperature nuclear matter properties.[43–46] The framework has also been effectively extended to study hypernuclear systems.[23,47–49] However, the presence of finite-volume effects remains a significant challenge in extending NLEFT applications to critical nuclear systems such as the neutron-rich ^{6}He isotope, where the delicate balance of nuclear binding requires exceptional precision. This is another motivation for this work. According to the statement above, our workflow is presented in Fig. 1.

2. Samples Generation. The HLEFT is used to generate the model-independent samples of two identical boson systems. These samples are fed to symbolic regression, which is based on genetic algorithms (GA).[50,51] GA allows the computer to require fewer prior assumptions and provides a more flexible search space to find final expressions. Similar to the evolutionary processes in nature, GA employs mechanisms such as mutations and crossovers to generate new solutions. In this work, we use the famous PySR, which is a multi-population evolutionary algorithm with multiple evolutionary processes performed asynchronously. It uses a classic evolutionary algorithm for each cycle and tournament selection for individual selection. The details of the setup in PySR can be found in the Supplementary Materials (SM).

The challenge of finite volume extrapolation lies in long-range interactions,[6–9,12] especially when the range of force is comparable to the box size. Luckily, the extrapolation formula for the short-range potential can be obtained from Lüscher's formula for $\kappa L \gg 1$,[11] with κ the binding momentum and L the box size. Firstly, we regress the extrapolation formula for the short-range potential as a benchmark for the applicability of the PySR model. We work in a non-relativistic framework and consider two identical spinless particles with the same mass $m = 1969\,\text{MeV}$.* The short-range potential in coordinate space reads as

$$V(\boldsymbol{r}) = -C_0\delta^3(\boldsymbol{r})\,, \tag{1}$$

where $\boldsymbol{r}$ is the relative distance between the two particles, C_0 is the strength of the potential for tuning the binding energy of the two-particle system. The minus sign means an attractive potential. From the effective field theory point of view, the short-range potential $V(\boldsymbol{r})$ needs a physical cutoff to isolate the long-range contribution from the short-range one. Usually, a single-particle regulator,[52] $f(\boldsymbol{p}_1^{(\prime)}, \boldsymbol{p}_2^{(\prime)}) = \prod_{i=1}^{2} g_\Lambda(\boldsymbol{p_i}) g_\Lambda(\boldsymbol{p_i'})$, is applied, where $g_\Lambda(\boldsymbol{p}) = \exp(-\boldsymbol{p}^6/2\Lambda^6)$ is a soft cutoff function with $\boldsymbol{p_i}$ and $\boldsymbol{p_i'}$ the momenta of the incoming and outgoing ith particle.[23] Thus, the Hamiltonian can be written as

$$H = \sum_{i=1}^{2} \frac{\boldsymbol{p_i^2}}{2m_i} + f(\boldsymbol{p}_1^{(\prime)}, \boldsymbol{p}_2^{(\prime)}) V(\boldsymbol{q})\,, \tag{2}$$

*The polarization of non-zero spin particles would modify the finite-volume extrapolation formula, which will not be discussed in this manuscript.

in which m_i is the mass of the ith particle, $\boldsymbol{q} = \boldsymbol{p} - \boldsymbol{p}'$ is the transferred momentum of the two particles and $\boldsymbol{p}$ ($\boldsymbol{p}'$) represents relative incoming (outgoing) momentum between $\boldsymbol{p}_1$ ($\boldsymbol{p}_1'$) and $\boldsymbol{p}_2$ ($\boldsymbol{p}_2'$). The corresponding potential in momentum space $V(\boldsymbol{q}) = -C_0$ can be obtained by a Fourier transform from the expression in coordinate space.

The Schrödinger equation is written as

$$H_L\psi = E_L\psi, \tag{3}$$

where H_L and E_L are the Hamiltonian and the binding energy in a cubic box L^3. The solution of Eq. (3) can be written explicitly in a single-particle basis $|\psi\rangle = |n_1, \cdots, n_N\rangle$,[44] where n_i is an integer triplet specifying the lattice coordinates. The matrix exact diagonalization scheme uses the implicitly restarted Lanczos method to find the eigenvalues and eigenvectors[53] by SciPy[54] in Python. In order to study the finite volume extrapolation formula for short-range potential, we perform simulations on box sizes $L^3 = 10^3, 11^3, \cdots, 30^3\,\mathrm{fm}^3$ cubic lattice with two identical particles. The potential strength C_0 is set to 1.5, 2.0, 2.5, and $3.0\,\mathrm{MeV}^{-2}$ to generate the samples. With this setup, we can extract the energy E_L in finite volume by solving Eq. (3) for various cases. The details of the samples can be found in the SM.

The Yukawa potential,[6]

$$V(\boldsymbol{r}) = -C_{01}\delta^3(\boldsymbol{r}) - C_{02}\frac{\mathrm{e}^{-\mu r}}{r} \tag{4}$$

with $1/\mu$ reflecting the range of the force, is used to describe the long-range potential. Here, C_{01} and C_{02} are the strengths of the short-range potential (δ-potential) and the long-range potential (Yukawa potential). One notices that the short-range behavior of the Yukawa potential is divergent and needs regularization, which is the reason why the first term exists. For simplicity, we set $C_{01} = C_{02}$ and choose the values 0.03, 0.09, 0.12, and $0.21\,\mathrm{MeV}^{-2}$ to generate the samples. These values allow the binding energy of the two-body system with the long-range potential to be close to that with only the short-range potential. Only in this case can one isolate the role of the long-range potential on the finite-volume extrapolation formula. For the short-range term, the single-particle regulator $f(\boldsymbol{p}_1^{(\prime)}, \boldsymbol{p}_2^{(\prime)})$ is still applied. At the same time, for the long-range potential term, the regulator[†] $\hat{f}(\boldsymbol{q}) = \exp[-(\boldsymbol{q}^2 + \mu^2)/\Lambda^2]$ is applied.[5] The Hamiltonian H in this case can be written as

$$H = \sum_{i=1}^{2}\frac{\boldsymbol{p_i}^2}{2m_i} + f(\boldsymbol{p}_1^{(\prime)}, \boldsymbol{p}_2^{(\prime)})V_S(\boldsymbol{q}) + \hat{f}(\boldsymbol{q})V_L(\boldsymbol{q}). \tag{5}$$

Here, both the short-range potential $V_S(\boldsymbol{q}) = -C_{01}$ and the long-range potential $V_L(\boldsymbol{q}) \sim \frac{1}{\boldsymbol{q}^2+\mu^2}$ can be transformed into their coordinate forms by Fourier transformation. We perform simulations on box sizes $L^3 = 10^3, 11^3, \cdots, 30^3$ fm^3 cubic lattices. We set the potential strength $C_{01} = C_{02} = 0.03$, 0.09, 0.12, and $0.21\,\mathrm{MeV}^{-2}$ to obtain binding energies similar to those for only the short-range potential. The details can be found in the SM.

3. Symbolic Regression. We perform symbolic regression on the generated samples that characterize finite-volume effects. The PySR model[55] samples the space of analytic expressions defined by the set of operators, input variables, and constant terms for minimization through genetic programming. The pool of operations includes addition, subtraction, multiplication, division, exponential, logarithm, square, etc. The input variable is box size L. Unlike the massive data used in deep learning, a few samples should be sufficient in the PySR model. The model evolution process employs several mechanisms, such as mutations and crossovers, to generate new expressions. The algorithm performs mutations over 50 iterations of 50 different population samples, with each population containing 35 individuals. There are two elements to measure the goodness of the output formula in the PySR model, i.e., loss and score. The value of loss is used to measure how well the output formula describes the samples, which is defined as mean square error,

$$\mathrm{Loss} = \sum_{i=1}^{N}[E_{\mathrm{PySR}}(L_i) - E_{\mathrm{L}}(L_i)]^2/N\,. \tag{6}$$

Here, $E_{\mathrm{PySR}}(L)$ is the output formula of PySR model, $E_{\mathrm{L}}(L)$ is the energy at box size L^3 calculated from lattice effective field theory (LEFT). Score is used to estimate the form of the formula, which rewards minimal loss and penalizes the more complicated formula. It can be defined as

$$\mathrm{Score} = -\frac{\Delta\,\ln(\mathrm{Loss})}{\Delta\,C}. \tag{7}$$

Here, C is the complexity[‡] (its values can be found in the SM), which is defined as the total number of operations, variables, and constants used in a formula. The PySR model will consider both score, i.e., complexity and loss, to choose the best formula. The other parameters used in training process can be found in the SM.

The training process of symbolic regression is very similar to biological population inheritance. In initialization, the PySR model randomly provides several kinds of evolutionary frameworks, which are different from each other and are used as a starting point for a given evolution. Mutations and crossovers occur throughout each iteration. During each iteration, formulae will be produced and the PySR model will choose the best formula for the next iteration according to the value of loss and score. The iterations will stop until the loss and complexity reach the specified values set at the beginning. During this process, the PySR model will choose the best formula across all iterations.

4. Results. Based on the PySR model, we can perform a symbolic regression for the samples of the short-range attractive potential to find an expression that uniformly describes the finite-volume extrapolation. In the four cases

[†]Here, Λ is the cutoff to regularize the long-range potential, which is set equal to that for the short-range one above.

[‡]The upper limit of the C value can be set larger to allow higher order contributions as that in analytic analysis.[11]

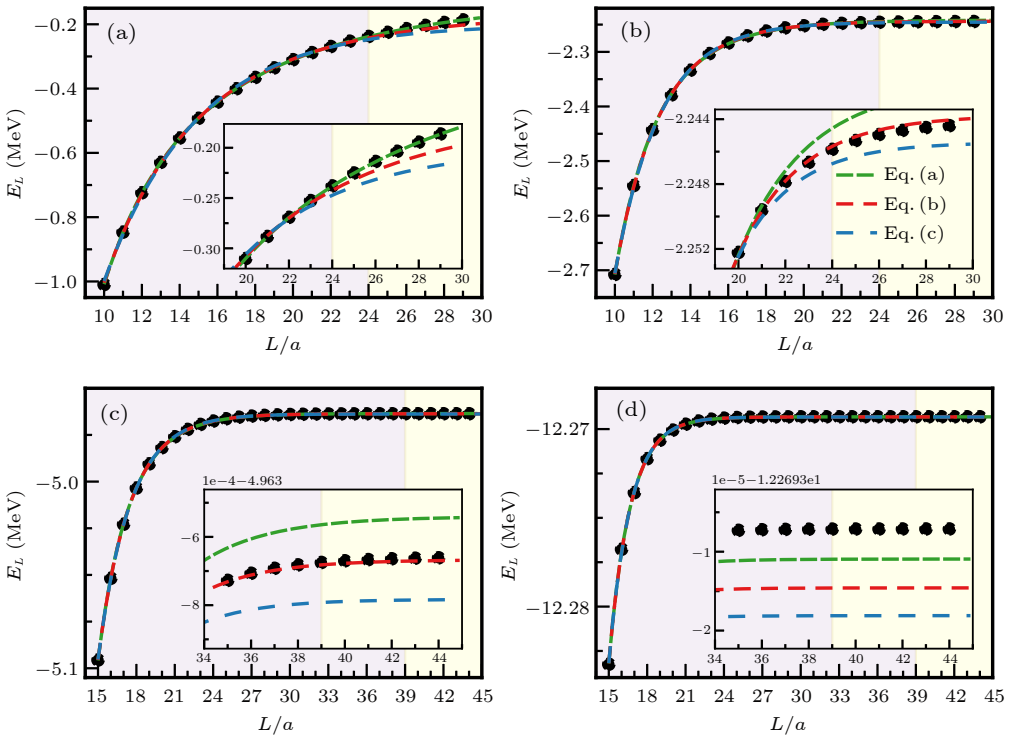

Fig. 2. The results of fitting the formula to samples. There are four cases of (a) $C_0 = 1.5\,\mathrm{MeV}^{-2}$, (b) $C_0 = 2.0\,\mathrm{MeV}^{-2}$, (c) $C_0 = 2.5\,\mathrm{MeV}^{-2}$, and (d) $C_0 = 3.0\,\mathrm{MeV}^{-2}$. Equations (a), (b), and (c) correspond to Eqs. (8a), (8b), and (8c), respectively. The box size L ranges from 10 to 30 fm. The purple region and the yellow region indicate the fitted and predicted areas by Eqs. (a), (b), and (c), respectively. Each graph has its own sub-graph to show greater detail of the lines between the fitted and predicted areas.

of C_0 values, three formulae are accepted by the PySR model,[§] as follows:

$$E_L = C_1 + C_2 \mathrm{e}^{-C_3 L}/L^2, \tag{8a}$$

$$E_L = C_1 + C_2 \mathrm{e}^{-C_3 L}/L, \tag{8b}$$

$$E_L = C_1 + C_2 \mathrm{e}^{-C_3 L}. \tag{8c}$$

In Fig. 2, we show the results of the three formulas fitting to the samples with the short-range potential, generated from LEFT. The purple area is the fitting region for the formulae derived from the PySR model. The yellow area is the predicted one. For the shallow bound state, e.g., Fig. 2(a), equation (8a) is the best choice. However, the volume size is not big enough to see the convergent behavior, making the regressed formula not universal. When the binding energy increases to a few MeV, i.e., Figs. 2(b) and 2(c), equation (8b) is better than Eq. (8a). When the binding energy further increases to more than 10 MeV, e.g., Fig. 2(d), all three formulae are good choices because their loss values are much smaller than those of the other subfigures of Fig. 2. As a result, we conclude that Eq. (8b) is the best regressed uniform formula to describe the samples with a few MeV binding energy.

The current well-established theoretical works [4,56–58] are based on the Lüscher formula [11] for the short-range potential with $\kappa L \gg 1$, where κ is the binding momentum of the two-body system. The energy shift of a shallow two-body bound state of identical bosons in finite volume is

$$E_L = E_\infty + \frac{C'}{L}\exp\left(-\kappa L\right), \tag{9}$$

where C' is the free parameter. This formula is exactly the form of Eq. (8b) regressed by PySR. In addition, the fitted values of the parameter C_3 in Eq. (8b) for the last three cases of Fig. 2 are equal to the binding momentum κ numerically. This also demonstrates that we have successfully regressed the finite-volume extrapolation formula for the short-range potential.

For the long-range potential, the strengths of the attractive potentials are set to obtain similar binding energies for the short-range potential. The range of the force parameter μ is set as $\mu = 20\,\mathrm{MeV}$ for these four C_0 cases. The other values of the force parameter and their effect on the finite-volume extrapolation will be discussed afterwards. The following three formulae[¶]

$$E_L = C_1 + C_2 \mathrm{e}^{-C_3 L}/L, \tag{10a}$$

$$E_L = C_1 + C_2 \mathrm{e}^{-C_3 L}, \tag{10b}$$

$$E_L = C_1 + C_2 \mathrm{e}^{-C_3 L} L, \tag{10c}$$

are accepted by the PySR model. Figure 3 shows the

[§]For the case of $C_0 = 1.5\,\mathrm{MeV}^{-2}$, the PySR model gives the formula $E_L = C_1' + C_2'/L + C_3'/L^2$. For the purpose of uniformity of the formula, when the ratio C_2'/C_3' is small enough, the formula is approximated as $E_L = C_1 + C_2 \mathrm{e}^{-C_3 L}/L^2$.

[¶]For the case of $C_{01} = C_{02} = 0.03\,\mathrm{MeV}^{-2}$, the PySR model gets the formula $E_L = C_1' + C_2'/L + C_3' L$. For the purpose of a uniform form of the formula, when the ratio C_3'/C_2' is small enough, the formula is approximated as $E_L = C_1 + C_2 \mathrm{e}^{-C_3 L}/L$.

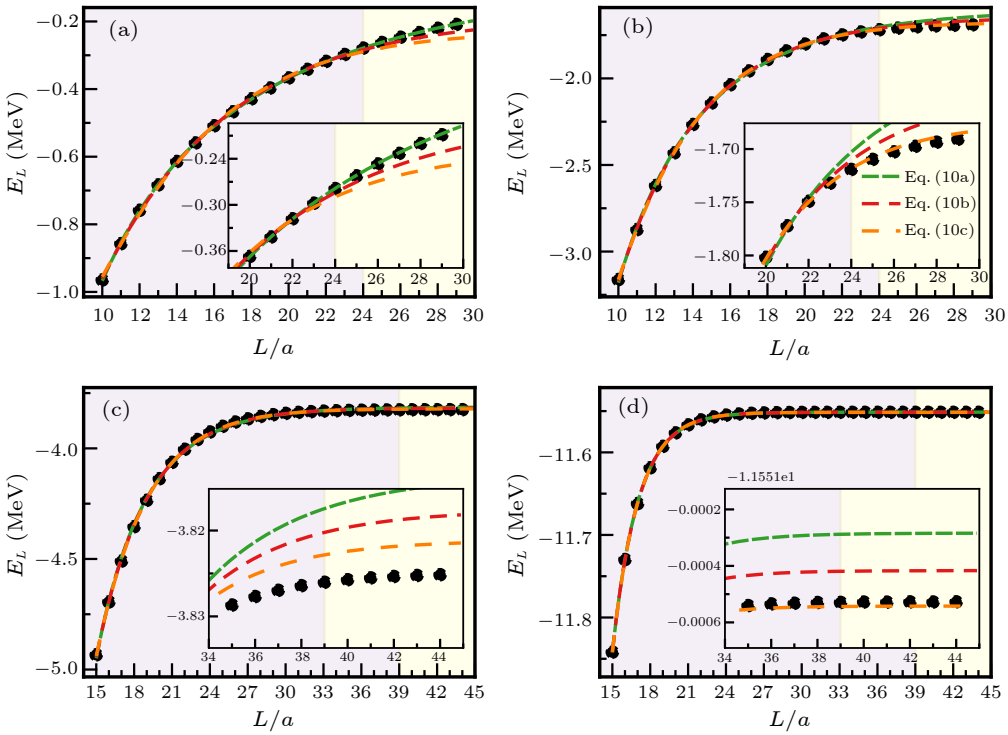

Fig. 3. The results of Eq. (10a) (green short dashed curves), Eq. (10b) (red dashed curves), and Eq. (10c) (orange long dashed curves) fitting to the samples of the long-range potentials with (a) $C_{01} = C_{02} = 0.03\,\mathrm{MeV}^{-2}$, (b) $C_{01} = C_{02} = 0.09\,\mathrm{MeV}^{-2}$, (c) $C_{01} = C_{02} = 0.12\,\mathrm{MeV}^{-2}$, and (d) $C_{01} = C_{02} = 0.21\,\mathrm{MeV}^{-2}$, respectively. The box size L ranges from 10 to 30 fm. The purple region and the yellow region indicate the fitted and predicted areas. Each graph has its own subgraph to show more details around the boundary between fitted and predicted areas. The black points are the samples generated from LEFT.

fitting results of the above three formulae to the energy with the long-range interaction. For the case with binding energy smaller than 1 MeV, i.e., figure 3(a), equation (10a) is preferred. However, the binding energy is too small to make the energy convergent in box size $30^3\,\mathrm{fm}^3$, making Eq. (10a) inapplicable to other cases. For the other cases, equation (10c) describes the samples very well and can be considered a uniform formula to describe the energy shift with the range of the potential as large as 10 fm. In comparison with the formula for the short-range potential, the power of L in front of the exponential becomes larger. This enlightens us that the power of L has a correlation with the range of the force. A theoretical formulation of the two-body quantization condition in the presence of a long-range force was proposed in Refs. [6–10,12]. We expect that a comparable power-law dependence on L can be obtained within the improved Lüscher formula.

As discussed above, the power of L in front of the exponential is related to the range of the force. Accordingly, we study the tendency of this power in the following. According to the results from the machine learning approach, the formula can be written in a general form,

$$E_L = C_1 + C_2 \mathrm{e}^{-C_3 L} L^n \,. \tag{11}$$

Here, n is an unknown parameter and needs to be fixed for various samples. The parameter μ in Eq. (4) is set as $10, 20, \ldots, 120, 400, 600, 800\,\mathrm{MeV}$ corresponding to the range of force $19.73, 9.87, \ldots, 1.64, 0.49, 0.33, 0.25\,\mathrm{fm}$. The first two ranges of force are compatible with the box size. As analyzed in the SM, the power of L in Eq. (11) decreases when the force range decreases. Moreover, when μ goes to infinity, i.e., the short-range interaction, the power n comes back to the formula $E_L = C_1 + C_2 \exp(-C_3 L) L^{-1}$ deduced from the Lüscher formula.[11] It indicates that no matter the form of the potential, the finite-volume extrapolation formula $E_L = C_1 + C_2 \exp(-C_3 L) L^{-1}$ can be reproduced once the range of force is short enough. On the other hand, when μ goes to zero, the power goes to infinity, which presents the behavior for the infinite long-range interaction (see the SM). The range of the force for the first two points of Fig. S2 of SM is compatible with the box size and cannot reflect the correct finite-volume behavior.

5. Summary and Outlook. Finite-volume extrapolation is an important step for extracting physical observables from lattice calculations. However, it is a significant challenge for systems with long-range interactions, especially when the range of the force is comparable to the lattice box size. Several theoretical works have been put forward to extract the finite-volume extrapolation formula based on the modified Lüscher formula numerically. To obtain an exact extrapolation formula, we employ symbolic regression for both short-range and long-range interactions. The samples are generated by the HLEFT and are fed to symbolic regression. As a benchmark, the finite-volume extrapolation formula for short-range interaction has been successfully regressed, i.e., the exponential form $\exp(-\kappa L)$ with the L^{-1} factor in front of it, which is in good agreement with the theoretical result. Furthermore,

we turn to the case of long-range interactions. The regressed results still keep the exponential form, but with the power of L dependent on the range of the force, i.e., the power of L decreases with the decreasing range of the force. When the range of the force becomes sufficiently small, the power converges to -1, recovering the short-range formula as expected. This agreement further validates the correctness of our extrapolation formula for long-range forces. Our work represents a significant advancement in leveraging machine learning to probe uncharted territories within particle physics.

Acknowledgments. We thank Serdar Elhatisari, Feng-Kun Guo, Ulf-G. Meißner, Andreas Nogga, and Akaki G. Rusetsky for their useful discussions on the finite volume dependence from the theoretical side. This work was supported in part by the National Natural Science Foundation of China (Grant Nos. 12375072, 12375073, 12275259, and 12135011). The work of Q.W. was also supported by Guangdong Provincial Funding (Grant No. 2019QN01X172). B.N. Lu is also supported by the National Security Academic Fund (Grant No. U2330401).

References

[1] Padmanath M and Prelovsek S 2022 *Phys. Rev. Lett.* **129** 032002

[2] Chen S, Shi C, Chen Y, Gong M, Liu Z, Sun W, and Zhang R 2022 *Phys. Lett. B* **833** 137391

[3] Lyu Y, Aoki S, Doi T, Hatsuda T, Ikeda Y, and Meng J 2023 *Phys. Rev. Lett.* **131** 161901

[4] Lüscher M 1986 *Commun. Math. Phys.* **105** 153

[5] Meng L, Baru V, Epelbaum E, Filin A A, and Gasparyan A M 2024 *Phys. Rev. D* **109** L071506

[6] Bubna R, Hammer H W, Müller F, Pang J Y, Rusetsky A, and Wu J J 2024 *J. High Energ. Phys.* **05** 168

[7] Dawid S M, Romero-López F, and Sharpe S R 2025 *J. High Energ. Phys.* **01** 060

[8] Romero-López F, Rusetsky A, Schlage N, and Urbach C 2021 *J. High Energ. Phys.* **02** 060

[9] Iritani T, Aoki S, Doi T, Hatsuda T, Ikeda Y, Inoue T, Ishii N, Nemura H, and Sasaki K 2019 *J. High Energ. Phys.* **03** 007

[10] Yu K, Wang G J, Wu J J, and Yang Z 2025 *J. High Energ. Phys.* **04** 108

[11] Lüscher M 1986 *Commun. Math. Phys.* **104** 177

[12] Meng L and Epelbaum E 2021 *J. High Energ. Phys.* **10** 051

[13] Schmidt M and Lipson H 2009 *Science* **324** 81

[14] Koza J R 1992 *Genetic programming: On the programming of computers by means of natural selection* ISBN 0262111705

[15] Amil N M, Bredeche N, Gagné C, Gelly S, Schoenauer M, and Teytaud O 2009 *A Statistical Learning Perspective of Genetic Programming*. In: Vanneschi L, Gustafson S, Moraglio A, De Falco I, Ebner M (eds) Genetic Programming. EuroGP 2009. Lecture Notes in Computer Science, vol 5481. Springer, Berlin, Heidelberg

[16] Cranmer M, Sanchez-Gonzalez A, Battaglia P, Xu R, Cranmer K, Spergel D, and Ho S 2020 arXiv:2006.11287

[17] Udrescu S M and Tegmark M 2020 *Sci. Adv.* **6** eaay2631)

[18] Tenachi W, Ibata R, and Diakogiannis F I 2023 *The Astrophysical Journal* **959** 99

[19] Dong Z, Kong K, Matchev K T, and Matcheva K 2023 *Phys. Rev. D* **107** 055018

[20] Makke N and Chawla S 2024 *PNAS Nexus* **3** 467

[21] AbdusSalam S, Abel S, and Crispim Romão M 2025 *Phys. Rev. D* **111** 015022

[22] Lu Y, Wang Y J, Chen Y, and Wu J J 2024 *Chin. Phys. C* **48** 073101

[23] Zhang Z, Hu X Y, He G, Liu J, Shi J A, Lu B N, and Wang Q 2025 *Phys. Rev. D* **111** 036002

[24] Lee D 2009 *Prog. Part. Nucl. Phys.* **63** 117

[25] Borasoy B, Epelbaum E, Krebs H, Lee D, and Meißner U G 2007 *Eur. Phys. J. A* **31** 105

[26] Epelbaum E, Krebs H, Lee D, and Meißner U G 2010 *Phys. Rev. Lett.* **104** 142501

[27] Epelbaum E, Krebs H, Lee D, and Meißner U G 2010 *Eur. Phys. J. A* **45** 335

[28] Lähde T A, Epelbaum E, Krebs H, Lee D, Meißner U G, and Rupak G 2014 *Phys. Lett. B* **732** 110

[29] Lu B N, Li N, Elhatisari S, Lee D, Epelbaum E, and Meißner U G 2019 *Phys. Lett. B* **797** 134863

[30] Lu B N, Li N, Elhatisari S, Ma Y Z, Lee D, and Meißner U G 2022 *Phys. Rev. Lett.* **128** 242501

[31] Elhatisari S, Bovermann L, Ma Y Z *et al.* 2024 *Nature* **630** 59

[32] Epelbaum E, Krebs H, Lähde T A, Lee D, Meißner U G, and Rupak G 2014 *Phys. Rev. Lett.* **112** 102501

[33] Shen S, Elhatisari S, Lähde T A, Lee D, Lu B N, and Meißner U G 2023 *Nature Commun.* **14** 2777

[34] Meißner U G, Shen S, Elhatisari S, and Lee D 2024 *Phys. Rev. Lett.* **132** 062501

[35] Shen S, Elhatisari S, Lee D, Meißner U G, and Ren Z 2024 arXiv:2411.14935

[36] Epelbaum E, Krebs H, Lee D, and Meißner U G 2011 *Phys. Rev. Lett.* **106** 192501

[37] Epelbaum E, Krebs H, Lähde T A, Lee D, and Meißner U G 2012 *Phys. Rev. Lett.* **109** 252501

[38] Epelbaum E, Krebs H, Lähde T A, Lee D, and Meißner U G 2013 *Phys. Rev. Lett.* **110** 112502

[39] Elhatisari S, Epelbaum E, Krebs H, Lähde T A, Lee D, Li N, Lu B N, Meißner U G, and Rupak G 2017 *Phys. Rev. Lett.* **119** 222505

[40] Zhang S, Elhatisari S, Meißner U G, and Shen S 2024 arXiv:2411.17462

[41] Bour S, Hammer H W, Lee D, and Meißner U G 2012 *Phys. Rev. C* **86** 034003

[42] Elhatisari S, Lee D, Rupak G, Epelbaum E, Krebs H, Lähde T A, Luu T, and Meißner U G 2015 *Nature* **528** 111

[43] Elhatisari S, Li N, Rokash A *et al.* 2016 *Phys. Rev. Lett.* **117** 132501

[44] Lu B N, Li N, Elhatisari S, Lee D, Drut J E, Lähde T A, Epelbaum E, and Meißner U G 2020 *Phys. Rev. Lett.* **125** 192502

[45] Ren Z, Elhatisari S, Lähde T A, Lee D, and Meißner U G 2024 *Phys. Lett. B* **850** 138463

[46] Ma Y Z, Lin Z, Lu B N, Elhatisari S, Lee D, Li N, Meißner U G, Steiner A W, and Wang Q 2024 *Phys. Rev. Lett.* **132** 232502

[47] Bour S, Lee D, Hammer H W, and Meißner U G 2015 *Phys. Rev. Lett.* **115** 185301

[48] Scarduelli V, Gasques L R, Chamon L C, and Lépine-Szily A 2020 *Eur. Phys. J. A* **56** 24

[49] Hildenbrand F, Elhatisari S, Ren Z, and Meißner U G 2024 *Eur. Phys. J. A* **60** 215

[50] Ireland D G, Janssen S, and Ryckebusch J 2004 *Nucl. Phys. A* **740** 147

[51] Fernández-Ramírez C, Moya de Guerrra E, Udías A, and Udías J M 2008 *Phys. Rev. C* **77** 065212

[52] Lu B N and Deng B G 2023 arXiv:2308.14559

[53] Lehoucq R B, Sorensen D C, and Yang C 1998 *ARPACK users' guide: Solution of large-scale eigenvalue problems with implicitly restarted Arnoldi methods* (Philadelphia, PA: SIAM)

[54] Virtanen P, Gommers R, Oliphant T E *et al.* 2020 *Nature Meth.* **17** 261

[55] Cranmer M 2023 arXiv:2305.01582

[56] Döring M, Hammer H W, Mai M, Pang J Y, Rusetsky T A, and Wu J 2018 *Phys. Rev. D* **97** 114508

[57] Hammer H W, Pang J Y, and Rusetsky A 2017 *J. High Energ. Phys.* **09** 109

[58] König S and Lee D 2018 *Phys. Lett. B* **77** 9